Journal of
Ceramic Science
and Technology

J. Ceram. Sci. Technol., **09** [3] 301-308 (2018)
DOI: 10.4416/JCST2018-00019
available online at: http://www.ceramic-science.com

The Corrosion of Mg-Partially Stabilized Zirconia During Service in Continuous Casting Tundish

K. Wiśniewska*, D. Madej, J. Szczerba

AGH University of Science And Technology, Krakow, Poland
received March 4, 2018; received in revised form June 3, 2018; accepted June 11, 2018

Abstract

One possible application for zirconium oxide is as a metering nozzle in a tundish for continuous steel casting. Such nozzles are mounted at the bottom of the tundish, and they are exposed to the corrosive effect of liquid steel at a temperature up to 1600 °C. In this study, the corrosion behavior of the zirconia metering nozzle after service in a tundish for continuous steel casting was investigated. The phase composition and chemical composition were investigated by means of x-ray diffraction and x-ray fluorescence, respectively. The microstructure of the nozzles was observed using a scanning electron microscope coupled with an energy-dispersive x-ray system. The major phases present in the metering nozzles were monoclinic zirconium oxide and Mg-stabilized zirconium oxide. With this investigation, it was possible to characterize the behavior of Mg-partially stabilized zirconia during steel casting. In each of the corroded nozzles, it was possible to distinguish two zones. The first zone was a light uncorroded area of the nozzle, and the second was a dark zone from the "hot face" of the nozzle. Furthermore, cracks along the surface of the brick were present in all corroded nozzles. SEM/EDS investigation confirmed that during the corrosion process liquid steel and inclusion infiltrate the zirconia nozzle.

Keywords: Mg-stabilized zirconia, corrosion, steel casting, refractories

I. Introduction

It is commonly known that there are three polymorphous forms of zirconium oxide: the stable monoclinic form at room temperature; up to about 1100 – 1200 °C monoclinicZrO_2 (m-ZrO_2) transforms into tetragonal ZrO_2 (t-ZrO_2). On further heating to above 2 300 °C, zirconium oxide transforms into a cubic ZrO_2 (c-ZrO_2).

A transformation from a tetragonal to monoclinic structure is associated with large volume change, of about 4.5 % [1,2]. The thermal expansion mismatch is related to microcracking during cooling [3]. To protect the ceramic material from failure, the zirconium oxide is partially or fully stabilized in a high-temperature structure. For this purpose, dopants as stabilizing agents such as MgO [4–6], CaO [7], Y_2O_3 [8], and CeO_2 [9] are used. Incorporating dopants into the zirconia structure creates the oxygen vacancies that neutralize the excess charge. H. Tomaszewski [10,11] shows that controlling the partial pressure of oxygen during heat treatment changes the phase composition of the zirconia material. The presence of metastable at room-temperature cubic (c) or tetragonal (t) phase in the non-stabilized zirconia materials sintered in reducing atmosphere is the result of oxygen non-stoichiometry [10].

Partially or fully stabilized zirconia is widely used as a thermal barrier coating on turbine plates to protect metallic components from heat, oxidation, and corrosion [12,13]. The zirconia-based material is also used in the steel industry as a nozzle in a tundish for continuous steel casting [14–16]. The nozzle provides the flow of molten steel in continuous steel casting and is exposed to liquid steel and inclusions as well as high temperature. The factors influencing the corrosion are molten steel and non-metallic inclusions, temperatures up to 1600 °C and rapid change of temperature.

The most important factor influencing the damage of partially or fully stabilized zirconia material is the loss of the stabilizing agent, which causes the phase deformation from cubic or tetragonal phase into monoclinic phase with volume increase.

Yanling Guo and others [17] investigated an effect of rare-earth oxides on corrosion by steel. At low temperatures, the reason for the degradation of the zirconia material was the dissolution of Fe_2O_3 in the zirconia structure. The stabilizing agent diffuses out of the zirconia and reacts with molten steel, which is the reason for phase transformation.

The destabilization process of yttria-stabilized zirconia is affected mostly by molten slag [18]. Slag components infiltrate the zirconia material and yttria is leached into the slag. The presence of SiO_2, Al_2O_3 and Fe_2O_3 also has an influence on the destabilization of Mg-stabilized zirconia. During the corrosion process, these components can be removed out of the zirconia structure and react with stabilizing agent [15,19]. Moreover, the porous structure of zirconia ceramic accelerates corrosion and increases the surface for corrosion attack [19].

* Corresponding author: kwis@agh.edu.pl

Cited studies have been conducted mostly under laboratory conditions. Zirconia-based materials applied in continuous steel casting is vulnerable to factors such as erosion by flowing molten steel, rapid temperature changes, infiltration of molten steel and slag into the porous ceramic and reducing atmosphere.

The aim of this study was the investigation of corrosion of the Mg-PSZ metering nozzle after service in a tundish for continuous steel casting for various corrosion test times. The knowledge of the behavior and material changes during service in a tundish can be the introduction to further investigation to improve material durability.

II. Experimental Methods

(1) Materials

The experimental procedure consisted of three steps. The first step was preparing the zirconia nozzle. For this purpose, Mg-partially-stabilized zirconia based on fine-grained material was used. The nozzle was formed by means of cold isostatic pressing and fired at 1640 °C to obtain the dense refractory material. The second step was the corrosion test in a tundish for continuous steel casting. The metering nozzle was mounted at the bottom of the tundish and exposed to the corrosive environment for 1 h and 30 min, 6 h and 30 min, 10 h and 30 min (for this paper the corroded nozzle was designated N1, N6, N10, respectively). The third step was analysis after service (*the post mortem analysis*) of the corroded material and comparison with an "as delivered" metering nozzle (designated N0). The grade of cast steel was B500SP/G, according to the Polish standard PN-H-93220:2006. The chemical composition of additives present in the cast steel was measured with spark optical emission spectroscopy. The analysis is presented in Table 1.

(2) Characterization

The bulk density and apparent porosity was measured with the Archimedes method. Phase identification was performed by means of the x-ray diffraction (XRD) technique, using a CuKα radiation on an X'Pert Pro diffractometer from PANalitycal with Bragg-Brentano geometry. The chemical composition was examined with the x-ray fluorescence (XRF) method. The Axios mAX wavelength dispersive x-ray fluorescence spectrometer from PANalytical was used for this study. The XRD patterns were refined with the Rietveld method, the Maud program [20,21] being used for this purpose. A scanning electron microscope (SEM) coupled with an energy-dispersive x-ray (EDS) system was used to observe the polished surface of the corroded and uncorroded nozzles. The ultra-high-definition NOVA NANO SEM 200 was used for this purpose.

III. Results

(1) Macroscopic observation and density

It was possible to distinguish three zones in each of the corroded nozzles. The first zone was a light uncorroded area of the nozzle, the second zone was a dark zone from the "hot face" of the nozzle, and the third zone was a black layer on the inner side of the nozzle. Fig. 1 presents a schematic drawing of the zirconia material after the corrosion test, and Fig. 2 shows the part of the zirconia nozzle after the 6.5-hours corrosion test. Furthermore, cracks along the surface of the brick in each of the corroded nozzles were present. The bulk

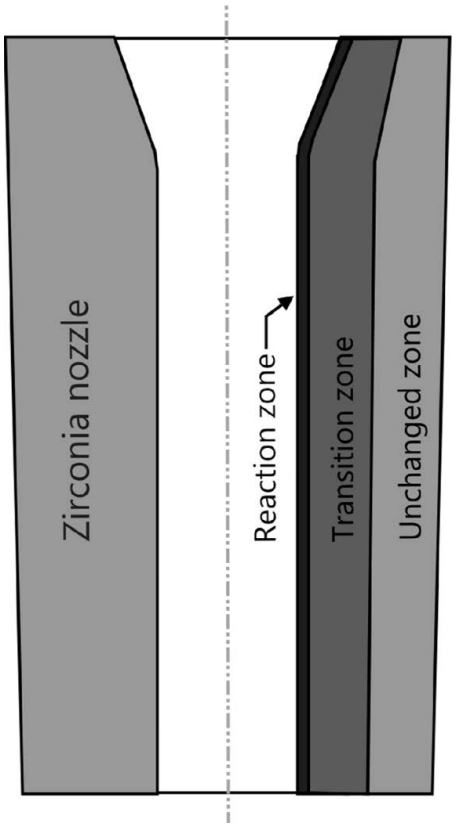

Fig. 1: Schematic drawing showing the zirconia nozzle, with distinguished zones: reaction, transition, unchanged.

Table 1: Chemical composition of additives in cast steel.

Steel grade	Content, mass%						
	C	Mn	Si	Al	P	S	Cu
B500SP/G	0.220	1.60	0.55	0.200	0.05	0.050	0.80
Measurement uncertainty	0.006	0.02	0.02	0.004	0.03	0.003	0.02

Fig. 2: Zirconia material N6 after the corrosion test for 6.5 hours.

density (Fig. 3a) changed slightly during the corrosion test, and a small increase in apparent porosity (Fig. 3b) could be observed. The apparent porosity of the zirconia material before the corrosion test (N0) was 7 %, and the bulk density was 5.34 g/cm^3. Changes in the bulk density are the resultant value between the infiltration by the compounds such as Al_2O_3, SiO_2, S or MnO, which can appear in cast steel as inclusions.

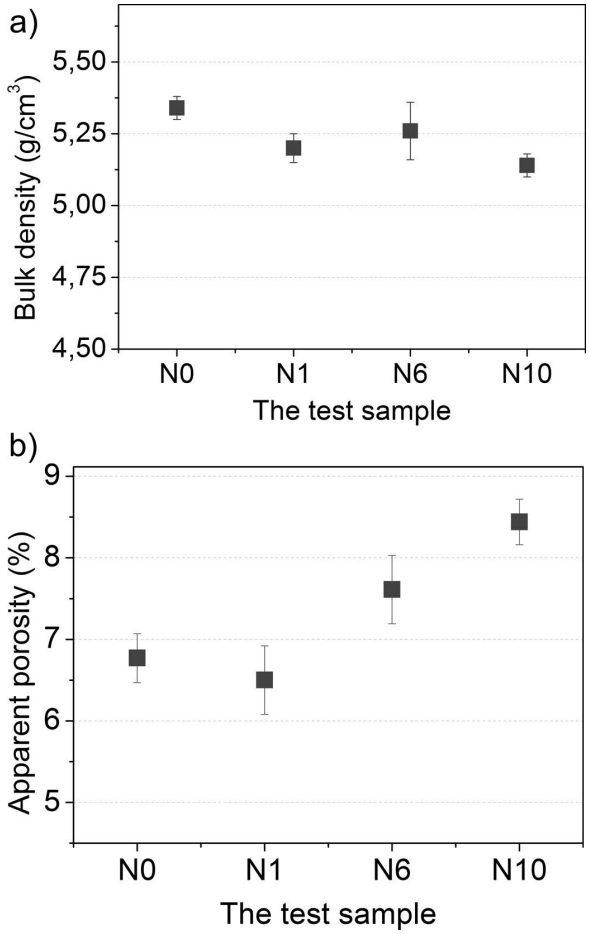

Fig. 3: a) The bulk density; b) The apparent porosity of the tested materials.

(2) Phase composition and chemical composition

The main phase present in the tested material is monoclinic zirconia (m-ZrO_2), and the second phase is cubic zirconia (c-ZrO_2) with the reflexes in the positions 2θ=30.4, 35.3, 50.6, 60, 62.9, 74.9 and 83°. It is worth noting that the intensity of reflexes derived from cubic zirconia increased in materials after the corrosion test. The XRD pattern is presented in Fig. 4.

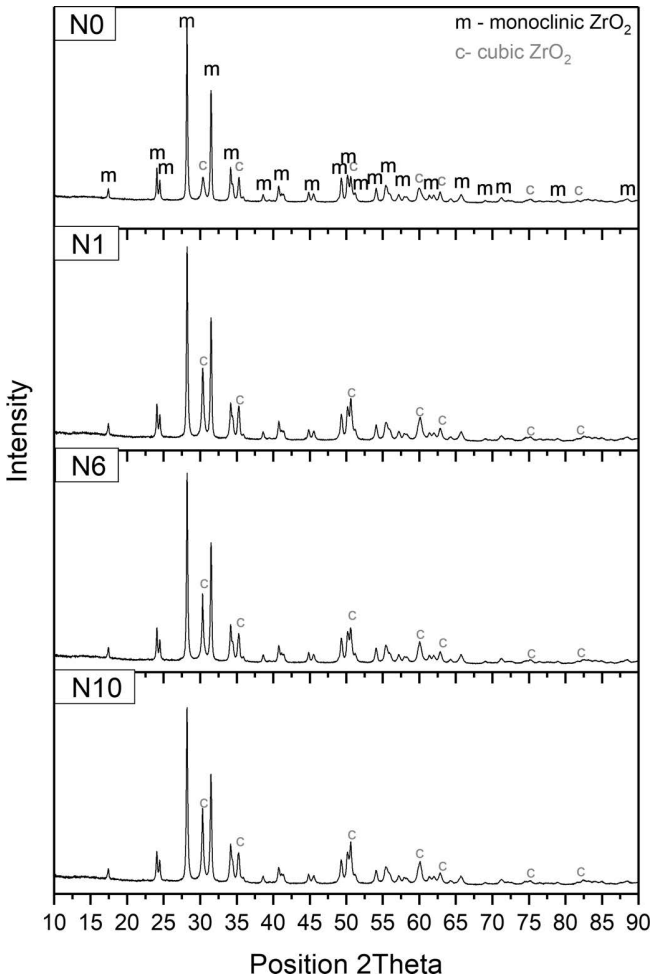

Fig. 4: The XRD patterns of samples N10, N6, N1, N0 (m-monoclinic zirconia, c-cubic zirconia).

The chemical composition changed during service. The content of oxides such as Al_2O_3, CaO, SiO_2 and Fe_2O_3 increased after 1.5 hours and 6.5 hours of the corrosion test, which is illustrated in Fig. 5. After 10.5 hours of the corrosion test, the content of these oxides was lower.

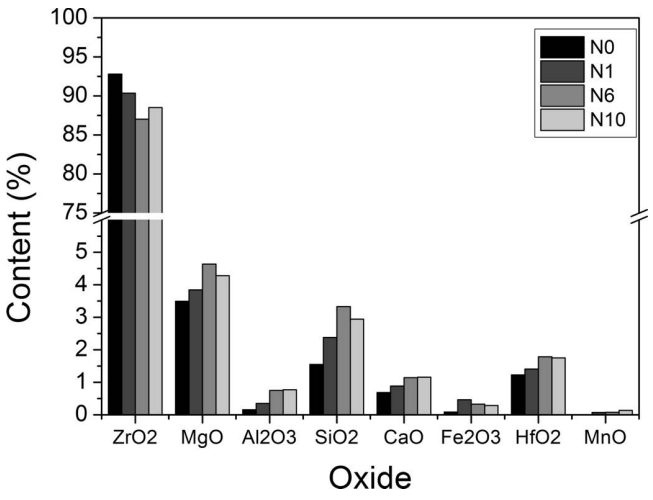

Fig. 5: Chemical analysis of the tested samples.

Especially, the content of SiO_2 increased significantly, from 1.55 % in sample N0 to 3.33 % in sample N6. Increasing those oxides is the result of the infiltration of the non-metallic inclusions during casting.

(3) Microstructure

Fig. 6 shows the cross-section of the polished surface of zirconia material before the corrosion test (the N0 sample). Grains of zirconium oxide are surrounded by silicate phase (dark gray). The EDS analysis confirmed that the chemical composition of this phase is similar to the composition of forsterite. Nevertheless, the content of forsterite was too low for reflexes to appear on the XRD pattern. Pores are also visible in this image, mostly between the grains.

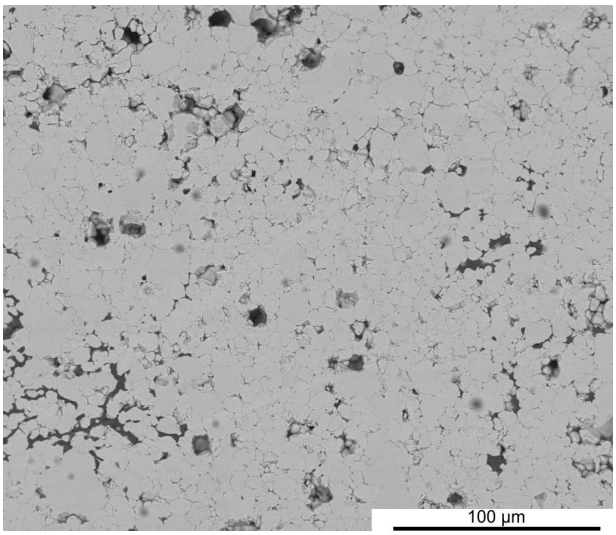

Fig. 6: Cross-section of the polished surface of the zirconia material (sample N0).

The microstructure of the zirconia material after the test changed, however, the changes occurred only in the inner area of the nozzle. In all corroded nozzles, it was possible to distinguish two areas. In the area from the working surface, the grains of zirconia were larger and microcracks extended through the zirconia grains. Fig. 7 shows the N1

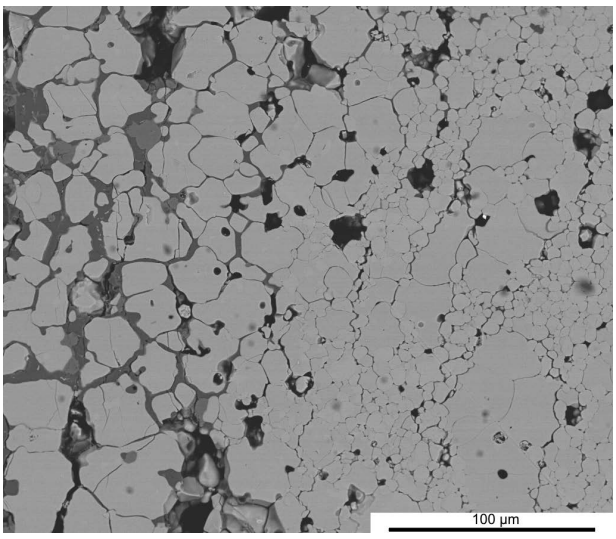

Fig. 7: Cross-section of the polished surface of the zirconia material (sample N1), the area from the ceramic/steel interface.

nozzle (after the corrosion test for 1.5 hours). Molten steel penetrated into zirconia material and created the drops of metal located in pores. Nevertheless, the main phase filling the pores is a SiO_2-rich phase.

In material N6 after the corrosion test for 6 and half hours (Fig. 8), microcracks and inclusions of steel are also visible.

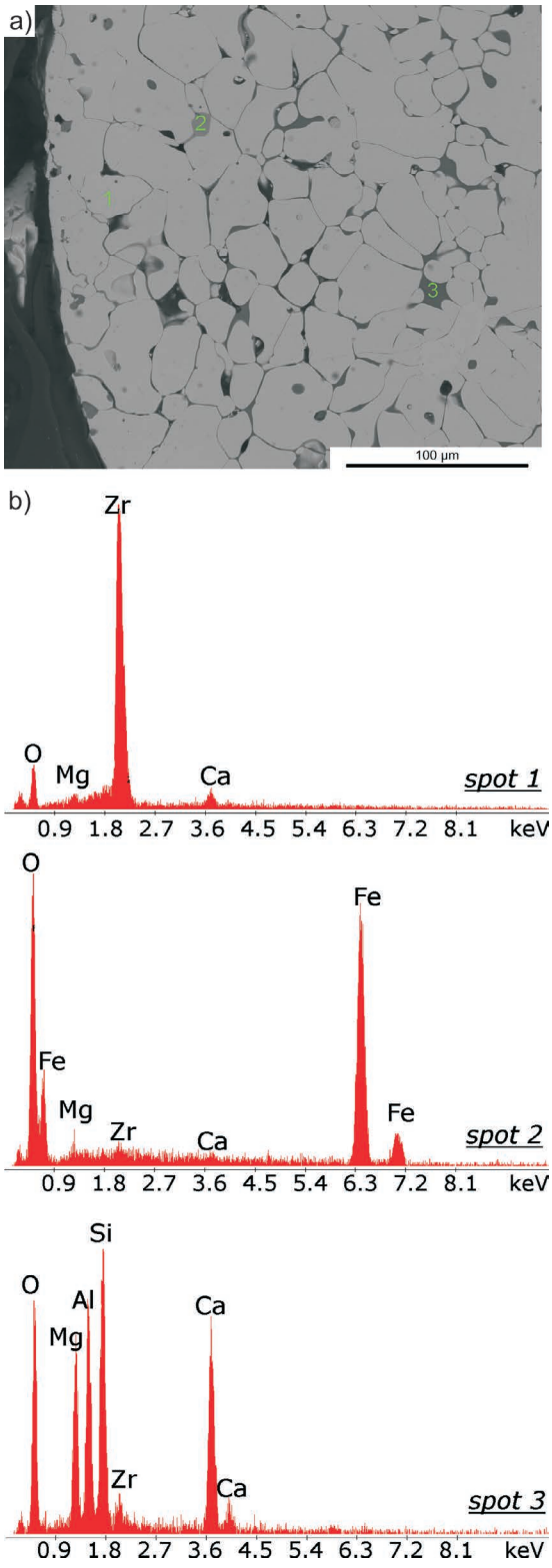

Fig. 8: a) Cross-section of the polished surface zirconia material (sample N6), the area from the ceramic/steel interface. Spot 1 - zirconium oxide, Spot 2 - iron, Spot - 3 Al and Si- rich phase; b) EDS analysis for selected spots.

The edges of the zirconia grains are rounded. Fig. 9 shows the cross-section of material N10, with a microcrack extending among the zirconia grains. Changes in the cross-section of the zirconia grains are the most significant. The grains are larger than in the samples discussed earlier, and it is difficult to distinguish the intergranular border. Slag and steel appear mostly as inclusions in the zirconia.

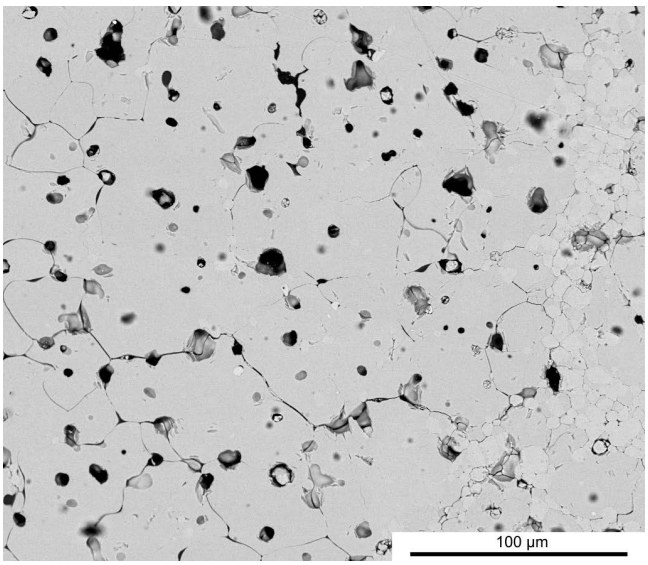

Fig. 9: The cross-section of the polished surface of zirconia material (sample N10), the area from the ceramic/steel interface.

Extending the test time increases the grain size and content of closed pores in the grains. In each tested sample after the corrosion test, the most significant changes in the grains' cross-section on the interface in contact with molten steel were noted. The microstructure changes with increasing distance from the working surface are shown in Fig. 10, based on the example of the N6 sample. The EDS analysis in 14 spots was performed to show the chemical composition changes in the zirconia grains. The grains of zirconia are noticeably larger in the reaction zone than in the transition zone. The thickness of the reaction zone measures approximately 300 µm. The quantities of magnesium and calcium are higher than in the transition zone, where the content of those elements drastically decreases. The appearance of iron and manganese was confirmed in the entire volume of the zirconia nozzle, and the content of these elements was constant in the reaction and transition zone, about 1 $\%_{at}$.

IV. Discussion

During service, the partially stabilized zirconia is exposed to temperature changes up to 1600 °C, a reducing atmosphere, contact with molten steel, and erosion by flowing steel.

The SEM investigation reveals that the microstructure changes are the most significant in the area in contact with the molten steel. In each tested material, the grains were bigger, and the shape was more regular. Steel and non-metallic parts of steel are located mostly between the zirconia grains, nevertheless, the EDS analysis showed that some amounts of iron and manganese had dissolved in zirconia. The average content of oxides in the zirconia grain from the area along the steel/ceramic interface is shown in Fig. 11.

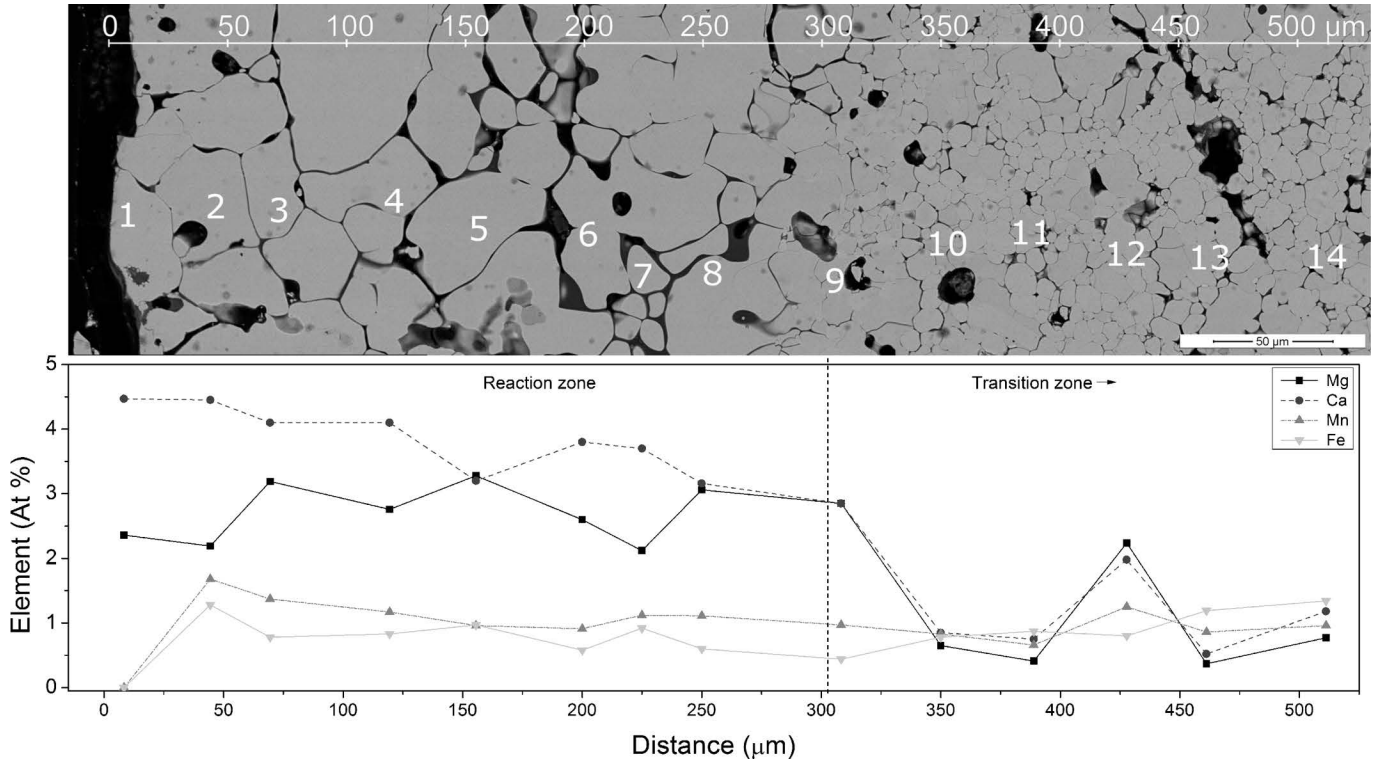

Fig. 10: The evolution of the microstructure in N6 nozzle from the reaction zone to the transition zone, with secondary element content at 14 spots.

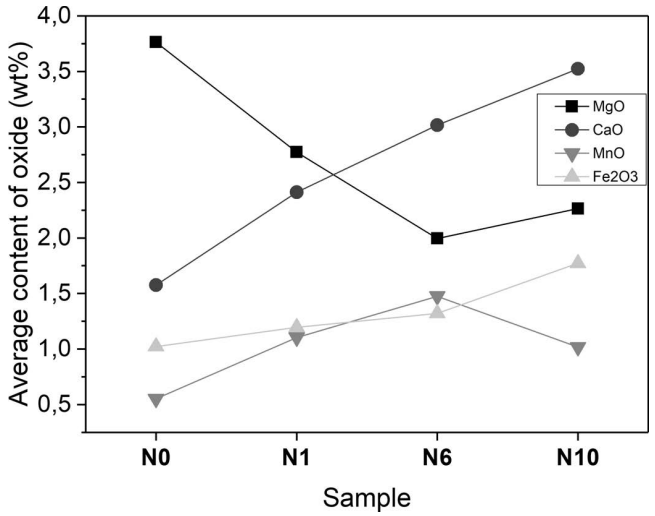

Fig. 11: The average content of selected oxide in zirconia grains along the ceramic/steel interface.

It is worth mentioning that the phase composition changed after the corrosion test. The content of c-ZrO_2 increases with the longer time of the corrosion test, which can be observed in the XRD patterns as an increasing intensity of the peak in position 2θ 30,4°, derived from Mg-stabilized ZrO_2. The Rietveld refinement [21] confirms the increasing content of c-zirconia. Table 2 compares the lattice parameters and phase content in each nozzle, the exemplary fitting is presented in Fig. 12. The lattice parameters of the monoclinic phase were unchanged, while in the cubic phase the *a*-parameter increased slightly with increasing time of the corrosion test. Doping a zirconium oxide with cations such as Mg^{2+} or Ca^{2+} (the ions have a size of 0.89 and 1.12 Å, respectively while Zr_{4+} is 0.84 Å [22]) is related to the formation of oxygen vacancies. The removal of the oxygen anions (O^{2-} has an ionic size 1.42Å) should reduce the volume of the unit cell. However, the introduction of larger cations into the zirconia structure causes an increase in volume. The earlier study [23] shows that the content of c-ZrO_2 is higher in the dark layer than in the light layer or in the reference sample. According to the EDS investigation, it can be assumed that not only magnesium cations incorporate into the zirconia structure but also calcium and iron cations.

Table 2: The unit cell parameters of the zirconium oxide.

	N0	N1	N6	N10
Goodness of fit	*1.53*	*1.51*	*1.81*	*1.67*
Monoclinic (ZrO_2)				
a [Å]	5.152	5.153	5.154	5.153
b [Å]	5.207	5.206	5.207	5.207
c [Å]	5.320	5.320	5.320	5.320
alpha [°]	90.000	90.000	90.000	90.000
beta [°]	99.208	99.193	99.192	99.188
gamma [°]	90.000	90.000	90.000	90.000
Volume [Å^3]	142.717	142.717	142.772	142.744
Content [wt%]	88.3	85.1	84.6	84.0
Cubic ($Zr_{0.91}Mg_{0.09}O_2$)				
a [Å]	5.023	5.096	5.099	5.102
alpha [°]	90.000	90.000	90.000	90.000
Volume [Å^3]	126.733	132.339	132.573	132.807
Content [wt%]	11.7	14.9	15.4	16.0

As shown by Aneziris *et.al.* [19], a slag can remove the stabilizing agent out of the structure. Nevertheless, molten steel is not as an aggressive agent as a slag. Iron cations can partially dissolve in zirconia under a reducing atmosphere. Martensitic m→t transformation causes crack

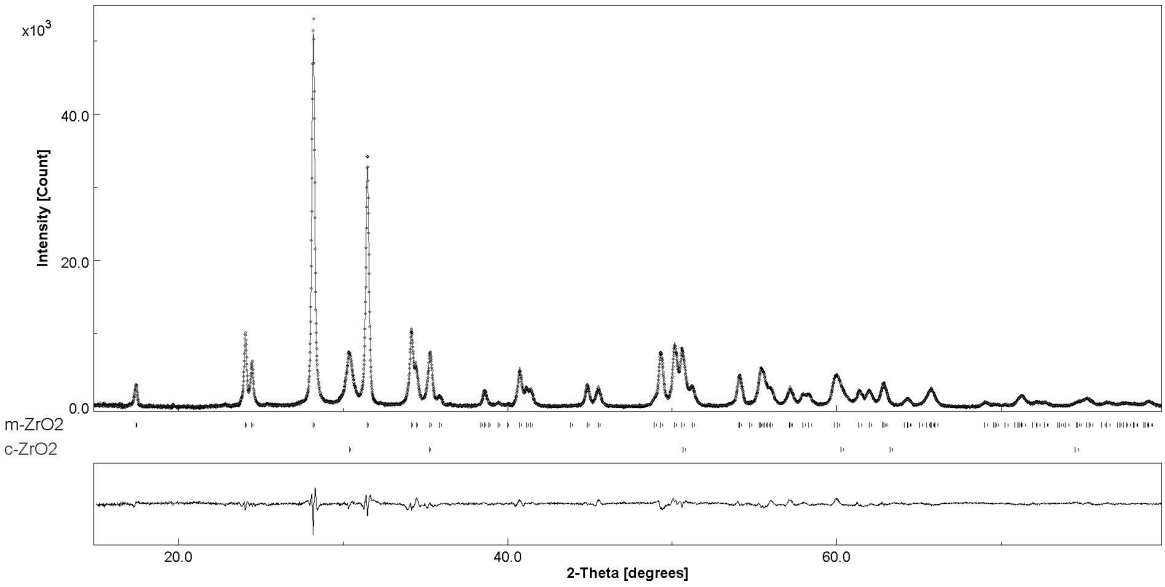

Fig. 12: The MAUD Rietveld plot for the reference nozzle (the N0 sample). The vertical lines mark the peaks of the phases included in the refinement.

formation, whereby the porosity increased which allowed the non-metallic part of steel such as silicon to penetrate into the zirconia material and accelerate the chemical corrosion and dissolution of the zirconia in the emerging glassy phase.

During service, the microstructure of the zirconia nozzle evolves. In the beginning, the material with the significant amount of monoclinic zirconium oxide is rapidly heated up to 1600 °C, which causes the m→t transformation, and further t→c transformation. The molten steel fills the pores in the reaction zone of the zirconia material. Iron and non-metallic part of steel partially dissolve in the ZrO_2 grains, which stabilizes the high-temperature structure of ZrO_2 after cooling. The grains of zirconia grow during corrosion test and the increasing time promotes the grain growth in the reaction zone.

Attention should be paid to the abrasion process that occurs on the inner layer of the zirconia material caused by flowing steel. During service, the zirconia material was continuously abraded, which causes the reaction zone to move into the material, nevertheless the thickness of this zone is constant. The grain growth causes the densification of material, therefore the infiltration process after 10 hours of service was slower, which was confirmed by XRF. In the N10 sample, the content of secondary oxides in the zirconia material was lower.

V. Conclusions

The corrosion of Mg-partially-stabilized zirconia ceramic was tested under industrial conditions in a tundish for continuous steel casting. The zirconia-based material was tested after service for different times.

From this investigation. the following conclusions are drawn:

a) During the corrosion test, molten steel and slag penetrate the zirconia materials. In the beginning, the slag fills the voids between the zirconia grains, while as the test time increased, the slag inclusions centered on the intergranular spaces.
b) At temperatures up to 1600 °C of the corrosion test, zirconia transformed into a high-temperature structure.
c) High temperature and rapid temperature changes lead to crack formation and failure.
d) Increasing the time of the corrosion test leads to more significant changes in the microstructure of the zirconia-based material.
e) Regardless of the test time, the most significant changes in the microstructure occur only in the area along the ceramic/steel interface.

Acknowledgements

This work was supported with Grant No. INNOTECH-K2/IN2/16/181920/NCBR/13 from the National Centre for Research and Development.

References

1 Kelly, J.R., Denry, I.: Stabilized zirconia as a structural ceramic: an overview, *Dent. Mater.*, **24**, 289 – 298, (2008).
2 Kisi, E.H., Howard, C.J.: Crystal Structures of Zirconia Phases and their Inter-Relation. *Key Eng. Mater.*, 153 – 154, 1 – 36, (1998).
3 Sibil, A. *et al.*: Microcracking of high zirconia refractories after t → m phase transition during cooling: An EBSD study. *J. Eur. Ceram. Soc.*, 31, 1525 – 1531, (2011).
4 Ikuma, Y., Yoshimura, A., Ishida, K., Komatsu, W.: Phase transformation and toughening in MgO dispersed with ZrO_2. in Tailoring Multiphase and Composite Ceramics 295 – 304 (Springer US, 1986). doi: https://doi.org/10.1007/978-1-4613-2233-7_22
5 Muccillo, E.N.S., Tadokoro, S.K., Muccillo, R.: Physical characteristics and sintering behavior of MgO-doped ZrO_2 nanoparticles, *J. Nanoparticle Res.*, **6**, 301 – 305, (2004).
6 Grain, C.F.: Phase relations in the ZrO_2-MgO system, *J. Am. Ceram. Soc.*, **50**, 288 – 290, (1967).
7 Imran, A., Alam, S., Irfan, M., Farooq, M.: Micro structural study of plasma-sprayed zirconia-CaO thermal barrier coatings, *Mater. Today Proc.*, 2, 5318 – 5323, (2015).
8 Chen, C.-C. *et al.*: Growth of zirconia and yttria-stabilized zirconia nanorod arrays assisted by phase transition, *Cryst. Eng. Comm.*, **12**, 3664, (2010).
9 Duh, J.-G., Dai, H.-T., Hsu, W.-Y.: Synthesis and sintering behaviour in CeO_2-ZrO_2 ceramics, *J. Mater. Sci.*, **23**, 2786 – 2791, (1988).
10 Tomaszewski, H.: Influence of oxygen content in the sintering atmosphere on the C-T transformation of the unstable zirconium oxide in the corundum matrix – Part I, (in Polish), *Mater. Elektron*, 36 – 48, (1994).
11 Tomaszewski, H.: Influence of oxygen content in the sintering atmosphere on the C-T transformation of the unstable zirconium oxide in the corundum matrix – Part II, (in Polish), *Mater. Elektron*, 21 – 33, (1994).
12 Bhatty, M.B., Khalid, F.A., Khan, A.N.: Behavior of calcia-stabilized zirconia coating at high temperature, deposited by air plasma spraying system, *J. Therm. Spray Technol.*, **21**, 121 – 131, (2012).
13 Alfano, M., Di Girolamo, G., Pagnotta, L., Sun, D.: Processing, microstructure and mechanical properties of air plasma-sprayed ceria-yttria Co-stabilized zirconia coatings, *Strain Int. J. Exp. Mech.*, **46**, [5], 409 – 418, (2010).
14 Bui, A.-H., Park, S.-C., Chung, I.-S., Lee, H.-G.: Dissolution behavior of zirconia-refractories during continuous casting of steel, *Met. Mater. Int.*, **12**, 435 – 440, (2006).
15 Volceanov, E. *et al.*: Development of zirconia composite ceramics and study on their corrosion resistance up to 1600 °C, *Key Eng. Mater.*, **264 – 268**, 1739 – 1742, (2004).
16 Primachenko, V.V. *et al.*: Postservice analysis of zirconia nonswirl nozzles for intermediate ladles of a continuous casting machine, *Refract. Ind. Ceram.*, **44**, 1 – 3, (2003).
17 Guo, Y.L., Long, S.G., Telle, R.: Effect of dopants on the corrosion behaviour of zirconia by steel at high temperature, *Key Eng. Mater.*, **280 – 283**, 999 – 1004, (2005).
18 Hemberger, Y., Berthold, C., Nickel, K.G.: Wetting and corrosion of yttria stabilized zirconia by molten slags, *J. Eur. Ceram. Soc.*, **32**, 2859 – 2866, (2012).
19 Aneziris, C.G., Pfaff, E.M., Maier, H.R.: Corrosion mechanisms of low porosity ZrO_2 based materials during near net shape steel casting, *J. Eur. Ceram. Soc.*, **20**, 159 – 168, (2000).
20 Lutterotti, L., Bortolotti, M.: Object oriented programming and fast computation techniques in MAUD, a program for powder diffraction analysis written in java, *IUCr Compcomm Newsletter*, 43 – 50, (2003).
21 Maud program, version 2.55, http://www.ing.unitn.it/~luttero/maud/
22 Shannon, R.D.: Revised effective ionic radii and systematic studies of interatomie distances in halides and chalcogenides, *Acta Cryst.*, **32**, (1976).
23 Winiewska, K., Madej, D., Szczerba, J.: Corrosion of the refractory zirconia metering nozzle due to molten steel and slag, *Mater. Technol.*, **50**, 29 – 32, (2016).